Characterization of an Advanced LIGO Quadruple Pendulum System

by

Andrew C. Thomas

Submitted to the Department of Physics
in partial fulfillment of the requirements for the degree of

Bachelor of Science in Physics

at the

MASSACHUSETTS INSTITUTE OF TECHNOLOGY
[February 2004]
January 2004

Author .....
Department of Physics
January 16, 2004

Certified by .....
Nergis Mavalvala
Assistant Professor
Thesis Supervisor

Accepted by .....
Professor David E. Pritchard
Senior Thesis Coordinator, Department of Physics

Characterization of an Advanced LIGO Quadruple Pendulum System

by

Andrew C. Thomas

Submitted to the Department of Physics
on January 16, 2004, in partial fulfillment of the
requirements for the degree of
Bachelor of Science in Physics

Abstract

The Laser Interferometer Gravitational-wave Observatory (LIGO) measures relative displacements of the interferometer mirrors induced by passing gravitational waves (GWs). At low frequencies, typically below 30 Hz, seismic noise is the dominant noise source that limits the sensitivity with which GW-induced mirror displacements can be measured. To shield the mirrors from the seismically driven motion of the ground, they are suspended from pendula which are in turn mounted on optical platforms with vibration isolation systems.

The Advanced LIGO goal for strain sensitivity is factor of 10 to 15 lower than that for Initial LIGO. This requires improved seismic isolation techniques to reduce the seismic noise limit by this factor. This is being achieved in two ways: active vibration isolation of the optical platform on which the suspended mirrors are mounted; and suspension of the interferometer mirrors from the final stage of multiple pendula.

In this thesis we characterize the dynamics of a prototype quadruple pendulum system. The figure of merit in evaluating and improving the performance of the quadruple pendulum is the motion of the mirror at frequencies between 1 and 100 Hz. To determine this, it is necessary to measure the frequency response (transfer functions) of the mirror displacement to motion of the penultimate mass of the pendulum. We describe the construction of a sensing and actuation system used to measure the transfer functions between the third and fourth masses, toward the ultimate goal of exploring the possibilities of third-mass system control. The measured transfer functions were compared to theoretical predictions generated by a simplified computer simulation of the complex system.

Thesis Supervisor: Nergis Mavalvala
Title: Assistant Professor

Acknowledgments

The first and greatest thank you goes to my supervisor, Dr. Richard Mittleman, for his willingness to take me onto the suspensions group and for his willingness to deal with my areas of inexperience.

Also very important to this project are Jonathan Allen and Myron MacInnis for their instruction and assistance with electronic and mechanical matters, and to my thesis advisor Nergis Mavalvala for keeping the bootprint firmly affixed to my behind.

And while he was not involved in the LIGO project, the man who has been my partner in science and conversation in every lab class MIT has thrown at me, Shankar Mukherji, deserves my sincerest thanks, for showing me how to be a true scientist: with wisdom, excitement, and a strong urge to explore and experience the world.

Contents

List of Figures

Chapter 1

Introduction

The Laser Interferometric Gravitational Wave Observatory (LIGO) is a long term joint collaboration between scientists at the California and Massachusetts Institutes of Technology, as well as several other institutions across North America and the world. The aim of the project, in common with several other ventures across the globe, is fundamentally to detect gravitational waves emitted from astronomical phenomena as predicted by Einstein in the General Theory of Relativity, then to use this confirmation as a means of detecting other astronomical phenomena.

LIGO consists of two large-scale Michelson-Morley style interferometric apparatuses, in Livingston, Louisiana and Hanford, Washington. Light from a laser enters a beam splitter, and each beam traverses one of two vacuum tunnels 4 km long and reflected by mirrors placed at each end. As gravitational waves pass through the apparatus, the relative displacements of the mirrors changes by a very small amount. We measure this change through the use of the interferometer itself; it is the length of the arms, combined with the short wavelength of the laser, that gives a high degree of sensitivity.

In order to make such a precise measurement of displacement, the apparatus must be shielded from all sources of noise. Seismic vibration is one such source. In order to deal with seismic noise, the mirror must be isolated from the ground's motion as sensitively as possible. This was accomplished in the first design stage (LIGO I) by suspending the mirror on an optical platform supported by a seismic isolation system.

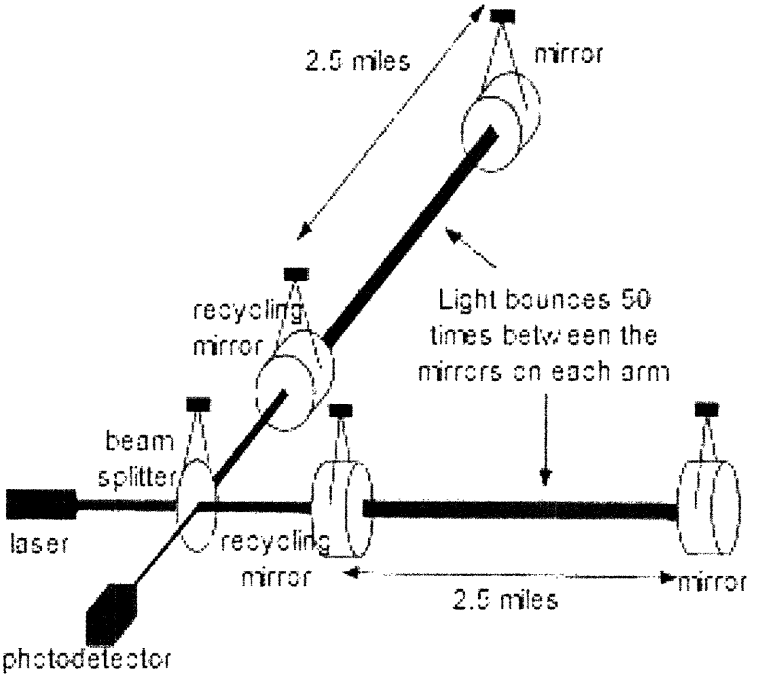

Figure 1-1: A schematic diagram of the LIGO interferometer, courtesy the Livingston Observatory.

The next refinement comes from placing the mirror on the final stage of a multiple pendulum; as the motion of one mass of a pendulum depends on the motion of the masses immediately above and below, the motion of the ultimate mass is isolated by several degrees from seismic noise, in much the same way as cascading filters in a series.

Recall that for a forced damped harmonic oscillator, the angular frequency response magnitude $A(\omega)$, determined by the oscillator equation

$$\ddot{x} + \beta\dot{x} + \omega_o^2 x = \frac{F}{m}e^{i\omega t}$$

is

$$A(\omega) = \frac{F/m}{\sqrt{(\omega_o^2 - \omega^2)^2 + (\beta\omega)^2}} = \frac{F/m}{\sqrt{\omega^4 - (2\omega_o^2 - \beta^2)\omega^2 + \omega_o^4}}$$

where β is the damping coefficient, ω_o is the undamped resonance frequency and F is the amplitude of the applied force. Above the apparatus's highest resonant frequency,

the ω^4 term dominates the damping and spring terms inside the square root. This gives a dependence of

$$A(\omega) \propto \frac{1}{\omega^2};$$

and so $A(f) \propto \frac{1}{f^2}$. It is worth mentioning that this dependence is equivalent to a drop in response of 12 dB over a factor of two in frequency (in other words, across an octave.) Moreover, if we have two restoring forces operating simultaneously – for example, if the driving force is applied to the first pendulum in a two-pendulum chain, there is a restoring force from the support and another from the second mass – we observe two f^{-2} dependences acting in concert, and will instead observe an f^{-4} dependence, or 24 dB per octave.

In generalizing to the multiple pendulum case, the uppermost resonance should exhibit this characteristic falloff. Since we wish to keep the ultimate mass of the pendulum still, it is critical to understand exactly how it moves in response to external forces, and then to use this information to construct an effective active damping system.

This approach is tested using two prototypical multiple-stage pendula, a three-mass pendulum at Cal Tech and a four-mass pendulum at MIT, the latter of these that we have used for this project. A pair of identical pendula is used, so that stabilizing forces can be applied between the two pendula, which are equally isolated from the ground. An active damping system, constructed of electromagnetic coils, permanent magnets and optical sensors, is constructed to operate between the third masses of each pendulum. This system is used to apply force to the system without coupling to the motion of the ground.

In Chapter 2 we proceed to describe the experimental setup. In Chapter 3, we present the experimental data and compare it to a simulated model, and discuss the results. We then present our conclusions and closing remarks in Chapter 4. We present supporting materials such as electronics and schematics in the Appendix.

Chapter 2

Apparatus

2.1 Quadruple Pendulum Design

The quadruple pendulum system consists of two identical chains, each with four masses. The main chain supports the interferometer mirror as the bottom-most mass, while the second chain provides reaction masses against which the masses of the main chain can recoil. Each chain is connected to the one below by piano wire. The bottom two (henceforth referred to as the third and fourth mass) are cylindrical, with their x axis pointed along the interferometer's optic axis, and are otherwise mechanically unremarkable[1]. The upper two masses are more elaborate; two elastically bending cantilever blades hold the wires that support the next lower mass (see figure 2-1.) These blades serve the purpose of isolating vertical motion in each pendulum.

Both pendulum chains are suspended from a support frame mounted on a seismic isolation system and housed in a vacuum chamber. The tests described in this thesis were performed at atmospheric pressure; future testing at higher sensitivity will have to be conducted under vacuum.

To ensure that the two pendulum chains are in vertical alignment, small objects can be added to a hole in the third mass to lower the chain. The total change in mass is small compared to the total, but the added stress on the cantilevers in the first and

[1]For the purposes of testing, the fourth mass has three holes placed equilaterally on the surface (see figure 2-1. These holes are designed to hold steel/aluminum inserts so that the mass and moment of inertia of the prototype mass will be identical to that of the final product.

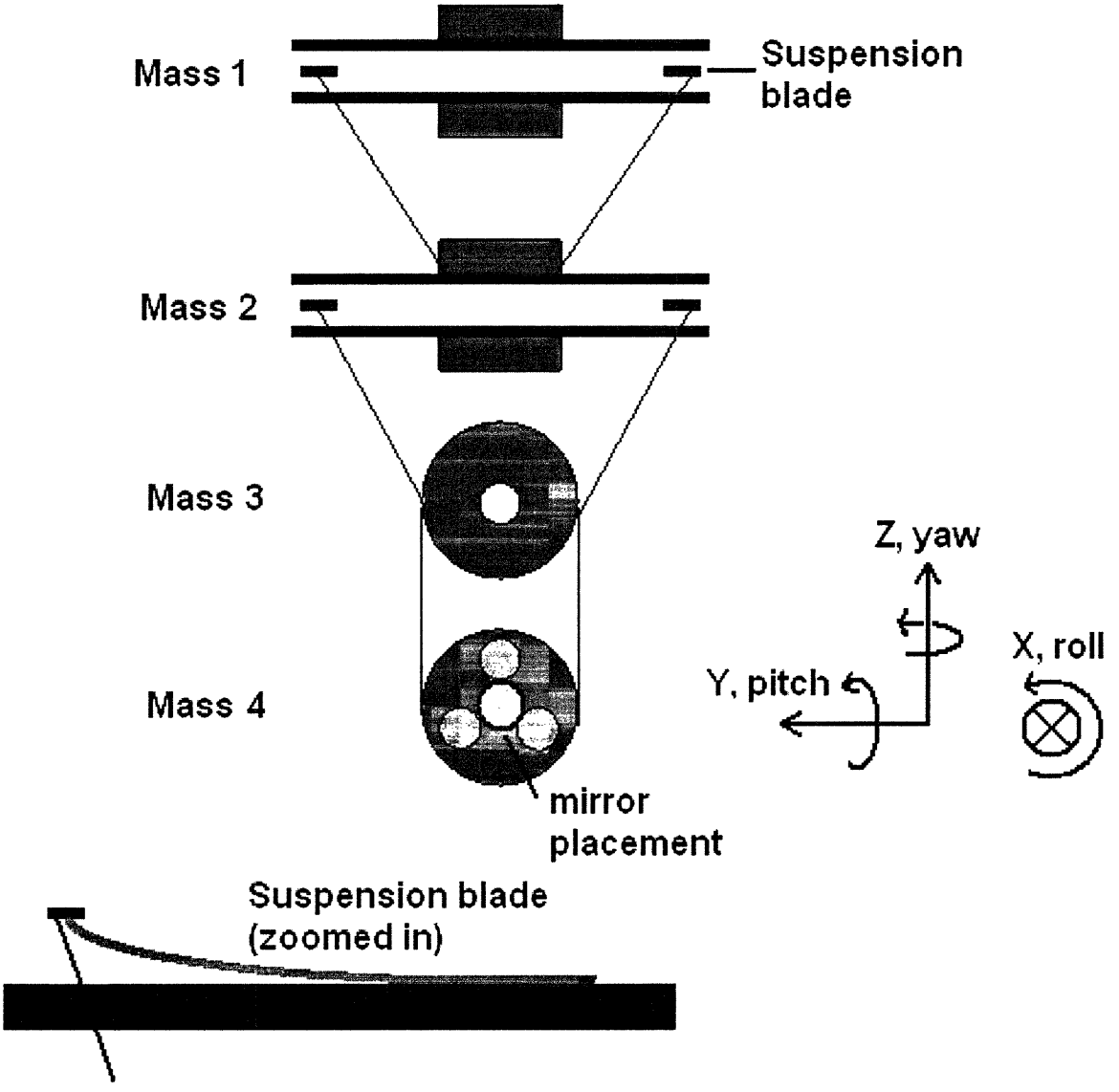

Figure 2-1: A schematic of the quad pendulum masses, including the sign convention to be used throughout the experiment. Just above is a diagram of the elastic blade on masses 1 and 2 used to suspend the next lower mass.

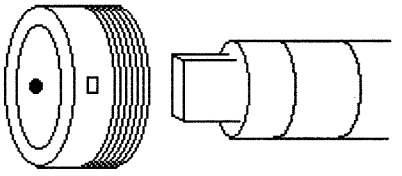

Figure 2-2: An OSEM assembly. On the left is the electromagnetic coil, with the infrared LED and photodiode placed on opposite sides. On the right is the permanent magnet attached to the flag.

second masses is significant to the pitch frequencies

2.2 Electronics

2.2.1 Optical Sensor/ElectroMagnetic Actuator(OSEM)

An OSEM is a custom sensing and actuation system that comprises an LED-photodiode pair for sensing and a current-carrying coil-permanent magnet for actuation[2]. The electromagnet itself is constructed of a plastic core wound with about 200 turns of copper wire and an approximate resistance of 12 Ω. Each is driven with a maximum current of 0.5 A, thus requiring 3 W of power per coil at maximum drive.

The optical sensing device is composed of an infrared LED paired with a photodiode sensitive to the LED frequency. By placing an opaque object in between the LED and photodiode, the amount of transmitted light varies. The voltage reading of the detector will then indicate the position of the object, known as a flag, within the coil assembly.

2.2.2 Alignment and Calibration

The OSEMs on the third mass were used to align the two pendulum chains. The zero position was chosen to be the point at which the observed voltage of the photodiode

[2]The permanent magnet is mounted on the mass to be actuated and is not part of the OSEM assembly itself.

was halfway between its maximum and minimum, a point that for alignment will not depend on the linearity of the detector.

This calibration point is found by measuring the maximum voltage, when the flag is completely removed from the OSEM, and the minimum voltage, when the flag is inserted as far as possible. As the flag is a flat piece of metal, it is inserted so that its face is normal to the direct line between the LED and photodiode (see figure 2-2).

Vertical alignment is also conducted by adding small metal objects to the third mass of one pendulum (the main chain) and manually adjusting the positions of the magnet on the other (the reaction chain). It is important to note that the addition of mass alters the equilibrium position of the cantilever blades and must be accounted for in the model.

2.2.3 Current Driver

The operation of the coils requires a linear current supply. I constructed a set of current drivers, tunable to a maximum output of $\pm$ 0.5 A with an input of $\pm$ 10 V, designed to match the voltage of a typical function generator. (See circuit diagram in appendix A.) At full strength, the heat dissipated by one of the drivers overloads the operational amplifier needed to drive the coil. As a result, extra heat sinks were constructed from raw aluminum to handle the load.

2.2.4 Primary (Third Mass) Damping

For our tests, the primary damping system actuation was applied between the third masses of each chain. This ensures that the force applied to one mass is equal and opposite to the force applied to the other, and because the pendula are designed to be identical, the effect is easily measurable.

Three OSEMs are used to drive the system, placed in an equilateral triangle about the center of the mass (see left panel of diagram 2-3.) The coils are mounted on one mass, the permanent magnets and flags onto the other. To detect the motion of the fourth mass, inductive position sensors are placed in a triangular pattern about the

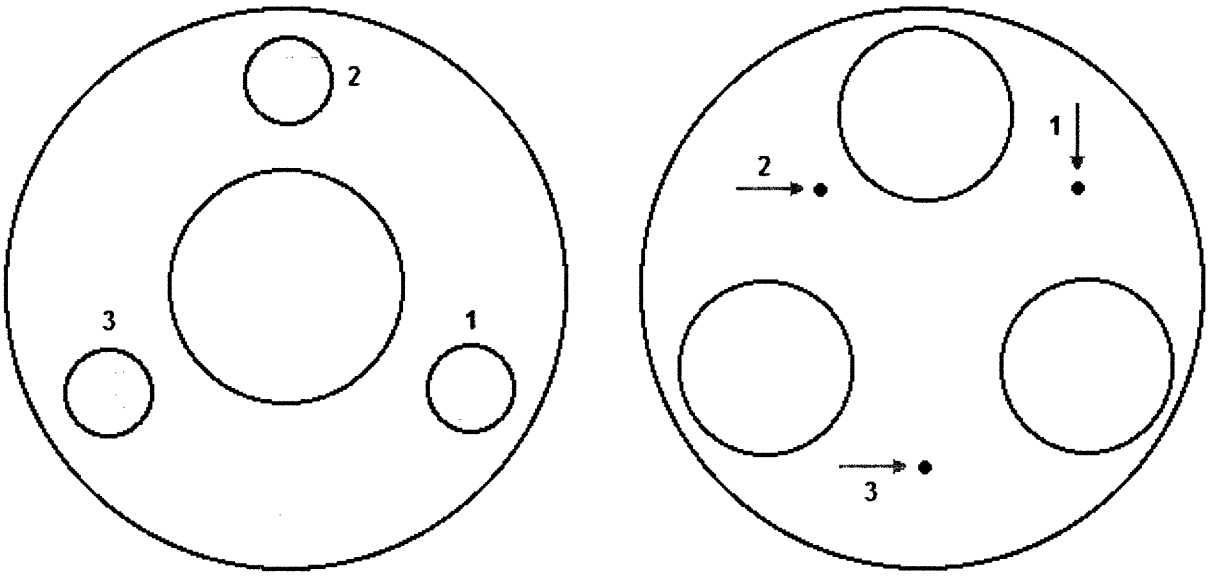

Figure 2-3: A diagram of the third (left panel) and fourth (right panel) masses. Coil placement is shown on the left, position sensors on the right. The view faces the outside of the mass; the coils are on the opposite face of the third mass.

center of the mass (see right panel of diagram 2-3.)

2.2.5 Secondary (First Mass) Damping

An additional damping system is installed on the first mass of each pendulum, connecting six OSEMs to the support ensuring that all six degrees of freedom can be damped.

The secondary damping system was built to damp 22 of the 24 modes of the quadruple pendulum through cross-coupling. Its hardware is entirely self-contained and is strong enough to effectively keep the first mass in place, if so desired. The damping system is never used at full strength as this would prove to convert the quadruple pendulum into an undamped triple pendulum swinging from a fixed object (coupled to the earth.)

The secondary damping was always on during our tests. This was necessary to reduce the ringing time (or Q) of the resonance of the upper pendula.

Chapter 3

Experiment

After constructing the hardware, we use the optical sensor to align the pendulum chains, and place the magnets with flags at a point such that the signal is at its median strength. We then drive the apparatus using swept-sine current drive and obtain the resulting transfer functions to the position sensors on the fourth mass.

3.1 Individual Coil Drive

The drive to the coils on mass 3 are controlled by two 4-channel SigLab control units, combined to allow for 8 total channels. For the bulk of testing, four position sensors were used; three placed in a triangular pattern on the fourth mass of one chain, the fourth at the center of the fourth mass of the second.

Insofar as the axes of coils are all in parallel, we are driving along only one axis. As a result, transverse motion (along the y axis) is not considered, nor is roll (rotation about the longitudinal axis) or vertical (translation along the z axis.) We thus consider the harmonic motion of each mass in three modes: translation along the x axis (longitudinal motion), and rotation about the y and z axes (pitch and yaw.)

The first stage of the experiment was executed by driving one coil at a time. This produces a response in the fourth mass which represents a summation of resonant modes though the profile depends on which coil was driven. This suggests an alternate means of finding frequency response: using the defined translational and rotational

modes of the pendulum as a driving pattern, as such a pattern should produce more output signal for the input mode.

3.2 Resonant Mode Coil Driving

Linear combinations of the three coil actuators on Mass 3 are used to drive the mass in position (L), pitch (P) and yaw (Y). Similarly, the sensors on Mass 4 can be combined to reconstruct the motion using the same three patterns of motion of the drive.

Given the equilateral placement of coils about the center of mass 3, each mode can be produced, with identical coils and magnets, as follows:

- Longitudinal: Coils 1, 2 and 3 have identical current and phase
- Yaw: Coils 1 and 3 have identical current and opposite phase
- Pitch: Coils 1 and 3 are identical in current and phase, 2 has double the magnitude and opposite phase

It was discovered that while coils 1 and 2 have a resistance of 12.2 Ω, coil 3 has a resistance of 13.0 Ω and hence a greater applied magnetic field for the same current. This serves to introduce a small amount of the other two modes when driving in the third; however, as it would be more than a factor of 10 smaller, it would not be enough to dominate resonances when driving and measuring the same mode. The magnets themselves are also not perfect; we expect an error of 10% in their strengths, which should not affect the resonant frequencies themselves.

Table 3.1: The geometric placement of each position sensor on mass 4, relative to the center.

Sensor	y position (cm)	z position (cm)
1	-6.1	7.0
2	10.6	7.0
3	0	-11.1

We wish to measure the resulting translational and angular modes in the motion of the fourth mass using the transfer functions of each position sensor. Since rotational

modes will be measured as angular functions, we require the perpendicular distance from the axis of rotation to the position sensor in question, which are given in table 3.1. Define y_n and z_n as the distance to sensor n from the z and y axes respectively. We can now relate the vector of observed transfer functions to each position sensor T_n to our chosen translational and angular modes, Longitude, Pitch and Yaw, using the transformation matrix A, defined as

$$\begin{pmatrix} T_1 \\ T_2 \\ T_3 \end{pmatrix} = A \begin{pmatrix} L \\ P \\ Y \end{pmatrix}$$

where

$$A = \begin{pmatrix} 1 & z_1 & y_1 \\ 1 & z_2 & y_2 \\ 1 & z_3 & y_3 \end{pmatrix} = \begin{pmatrix} 1 & 7.0 & 10.6 \\ 1 & 7.0 & -6.1 \\ 1 & -11.1 & 0 \end{pmatrix}.$$

The first column is dimensionless, as it represents translation; the second and third columns are in units of cm as they represent rotational radii. Care must be taken with regard to the units of the matrix elements, since the translational and rotational modes are in units of length and angle respectively.

In order to obtain our desired functions, we take the inverse of the matrix A to obtain

$$\begin{pmatrix} L \\ P \\ Y \end{pmatrix} = \begin{pmatrix} 0.2240 & 0.3893 & 0.3867 \\ 0.0202 & 0.0351 & -0.0552 \\ 0.0599 & -0.0599 & 0 \end{pmatrix} \begin{pmatrix} T1 \\ T2 \\ T3 \end{pmatrix}.$$

The transfer function for each position sensor is measured in volts to volts. The output voltage is converted to position through the properties of the position sensor, using a scale of 0.79 V/mm of motion. The input voltage is converted to a current at a ratio of 1 V/0.05 A (or 1 V/0.1 A for the top coil in the pitch drive) for each OSEM. A further step would involve converting the input current directly into the

applied force between the third masses.

3.3 Observations

Each data run was composed of four separate analyses compiled together by computer. This means that statistically, a coherence of $\sqrt{1/4} = 0.5$ is the minimum value for the data to be considered reliable.

Early data runs gave very poor values of coherence for the entire range of the data run. We hypothesize that this resulted from physical contact between the fourth mass and the position sensors, which was confirmed through visual inspection, running tests without the cover. To resolve this issue, the maximum driving voltage was reduced from 5 V to 2 V for individual coil runs, and a base voltage of 1 V for composite runs.

3.3.1 Inductive Coupling

The position sensors used for the test are inductive in nature. As a result, it is theorized that the magnetic drive of the coil is producing a signal in the position sensor purely due to the change in field, independent of position.

As a test, we clamp the apparatus down so that the fourth mass is unable to move and drive the system. We then drive one coil alone and measure the resulting transfer function (see figure 3-7). While coherence below 50 Hz was generally unacceptable, between 50 and 600 Hz the coherence is nearly unity. It is clear that there is an increase of approximately 6 dB per octave, which suggests a linear dependence of frequency to response. This verifies that there is an inductive effect which dominates after 50 Hz, severely limiting the operating range of the position sensors. As a result, further drive experiments were done below this frequency. Moreover, resonances below 1 Hz proved to overdrive the system. The drive was configured to run between 1 and 50 Hz.

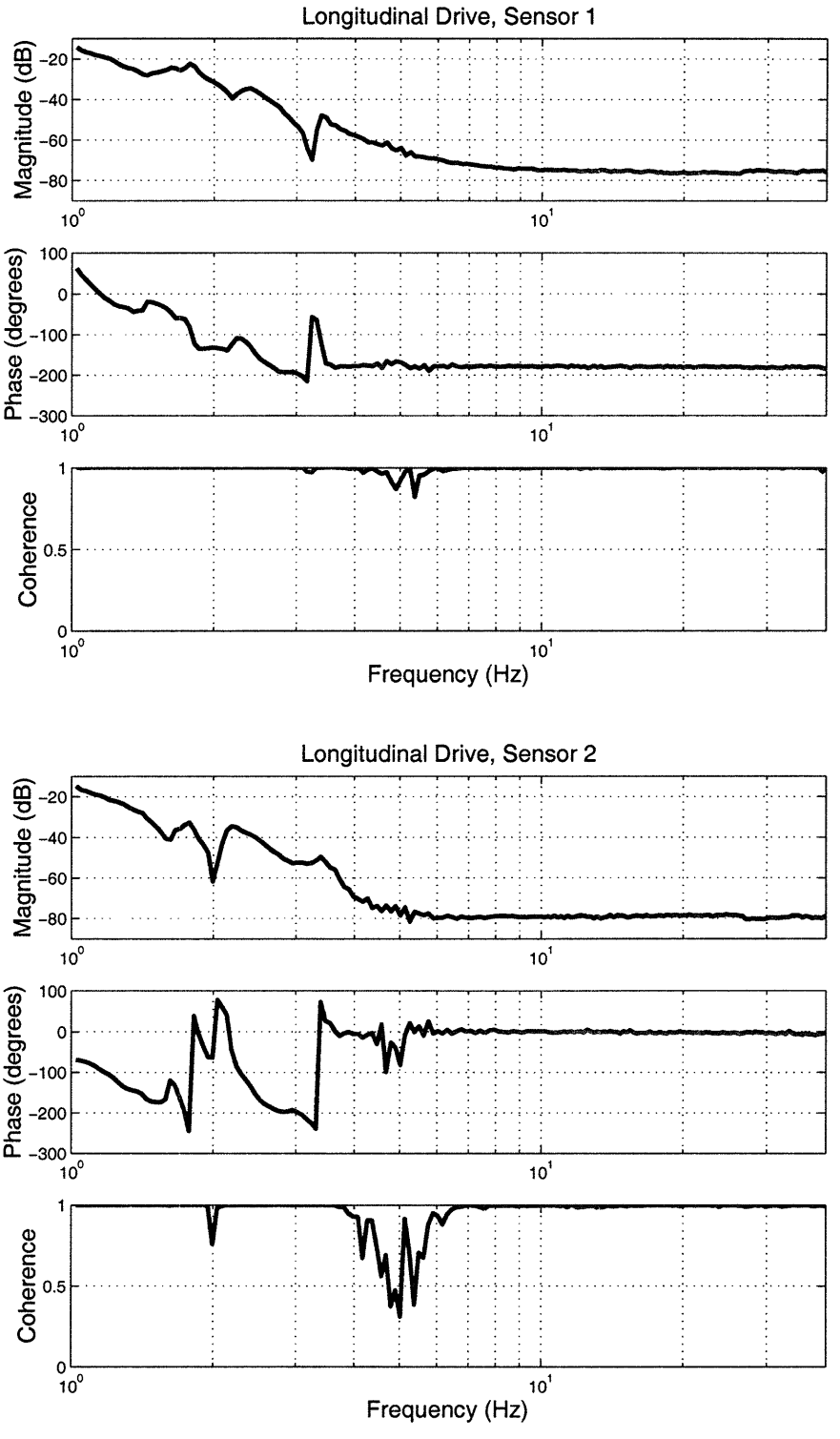

Figure 3-1: Longitudinal drive transfer functions for sensors 1 and 2.

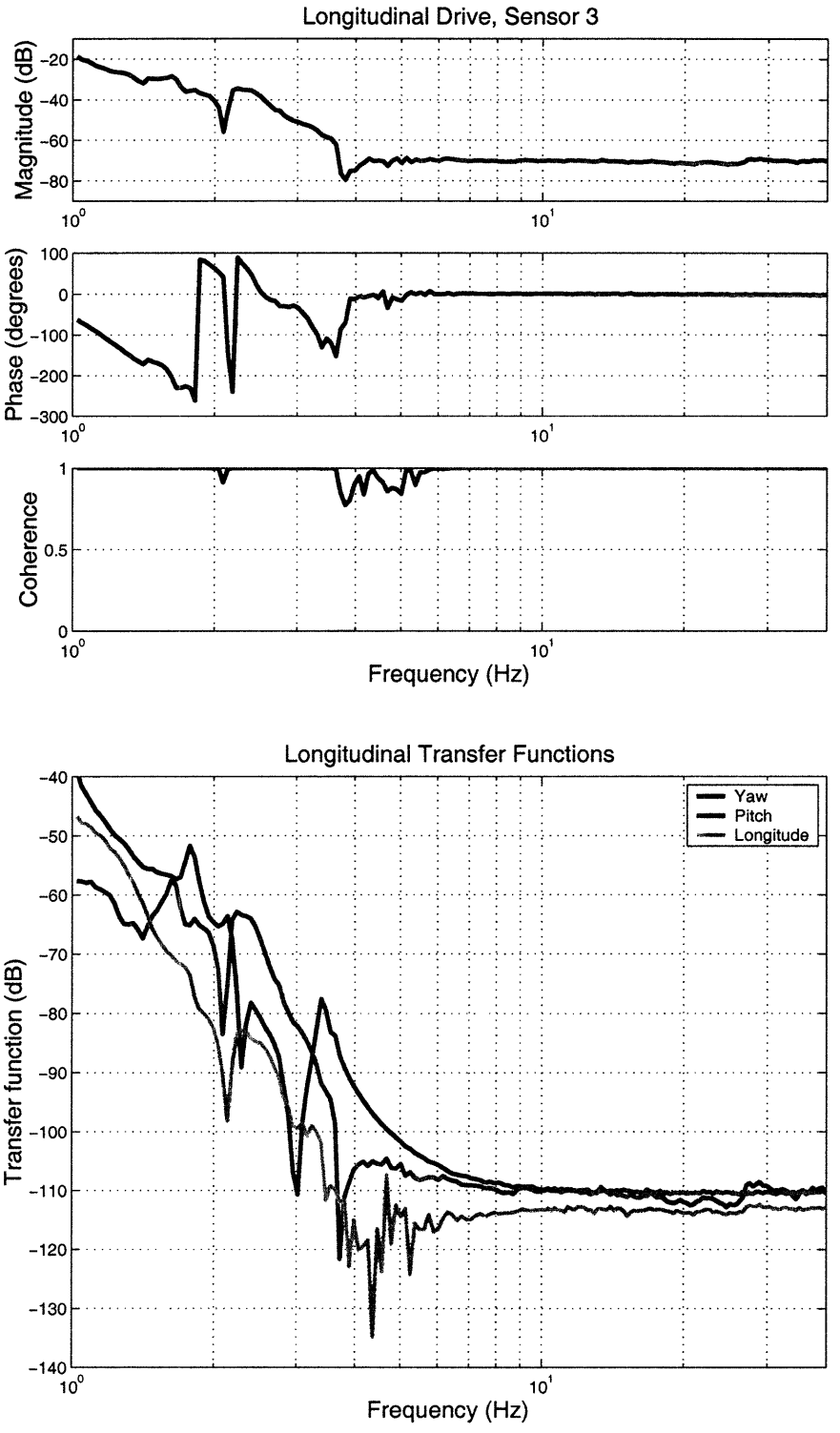

Figure 3-2: Longitudinal drive transfer function for sensor 3, and a graph of the transfer functions in terms of each composite mode.

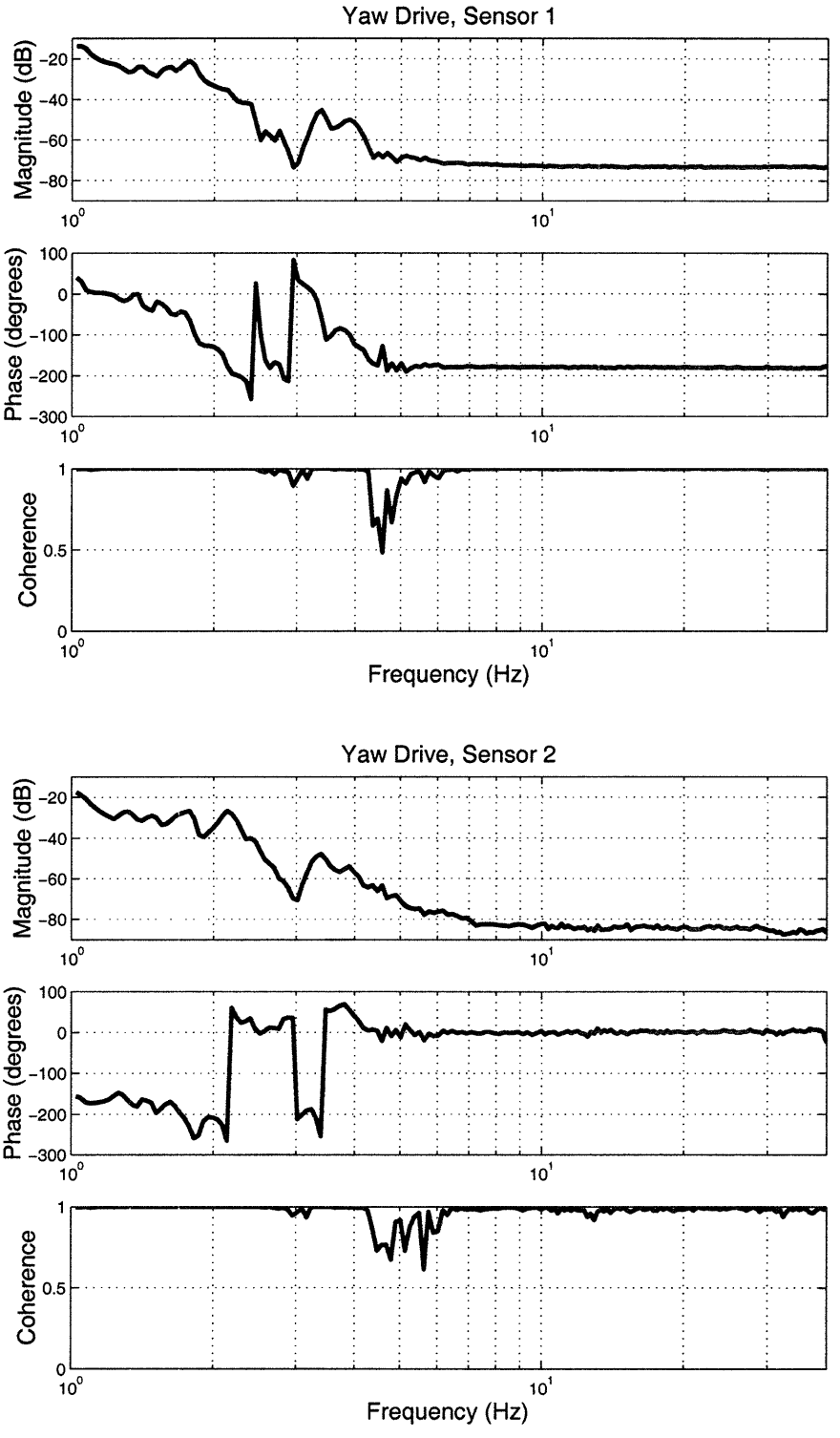

Figure 3-3: Yaw drive transfer functions for sensors 1 and 2.

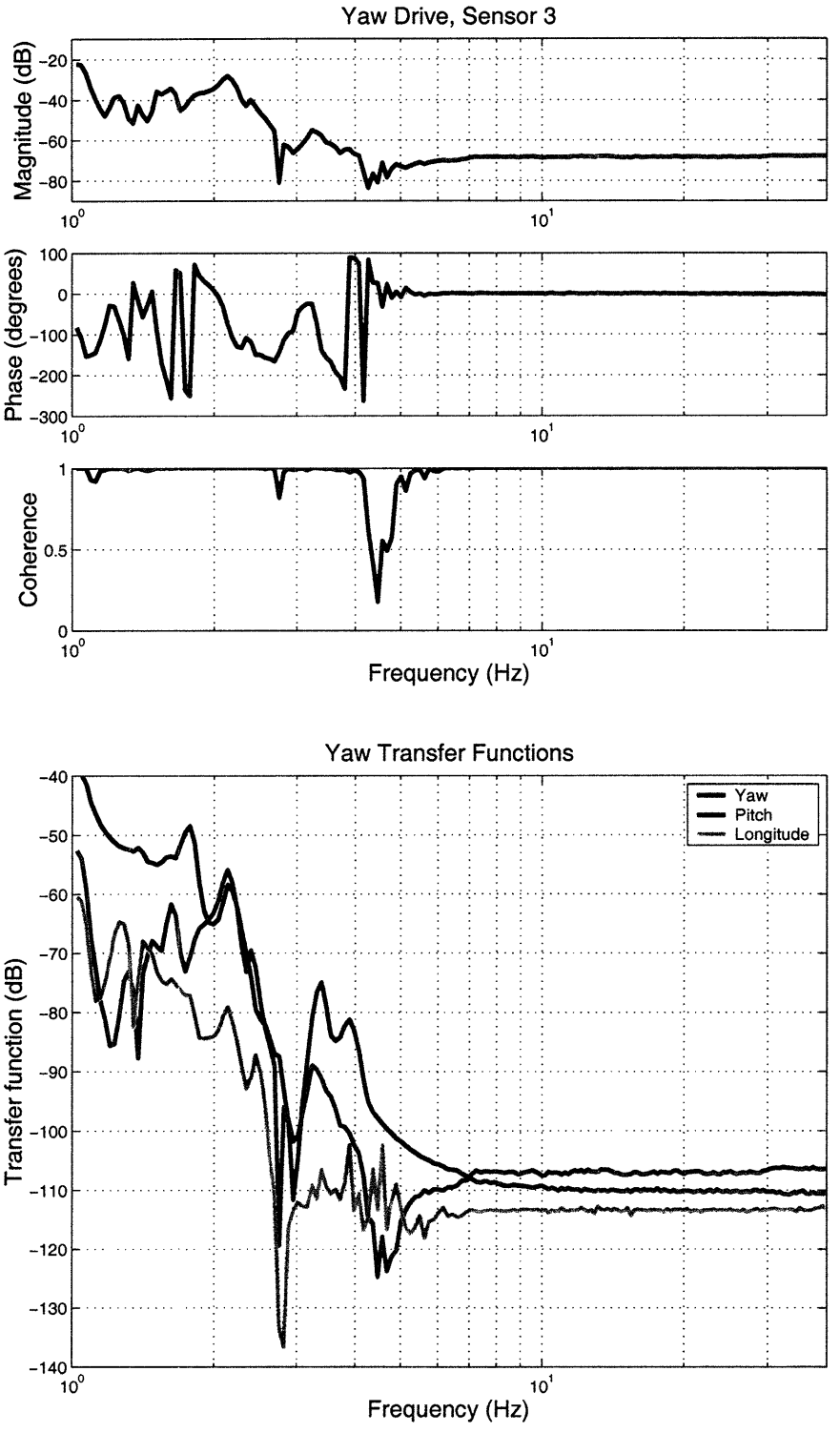

Figure 3-4: Yaw drive transfer function for sensor 3, and a graph of the transfer functions in terms of each composite mode.

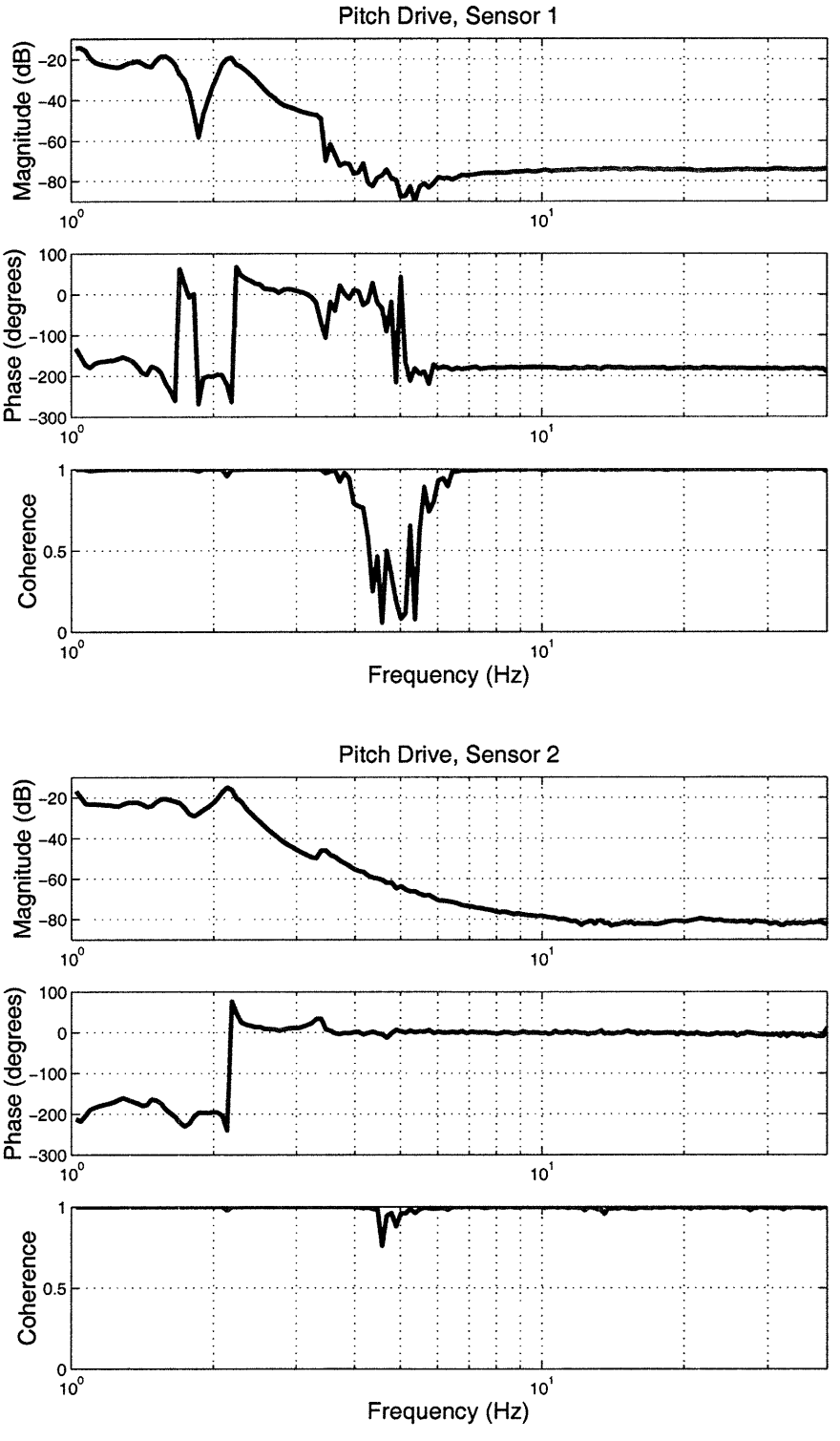

Figure 3-5: Pitch drive transfer functions for sensors 1 and 2.

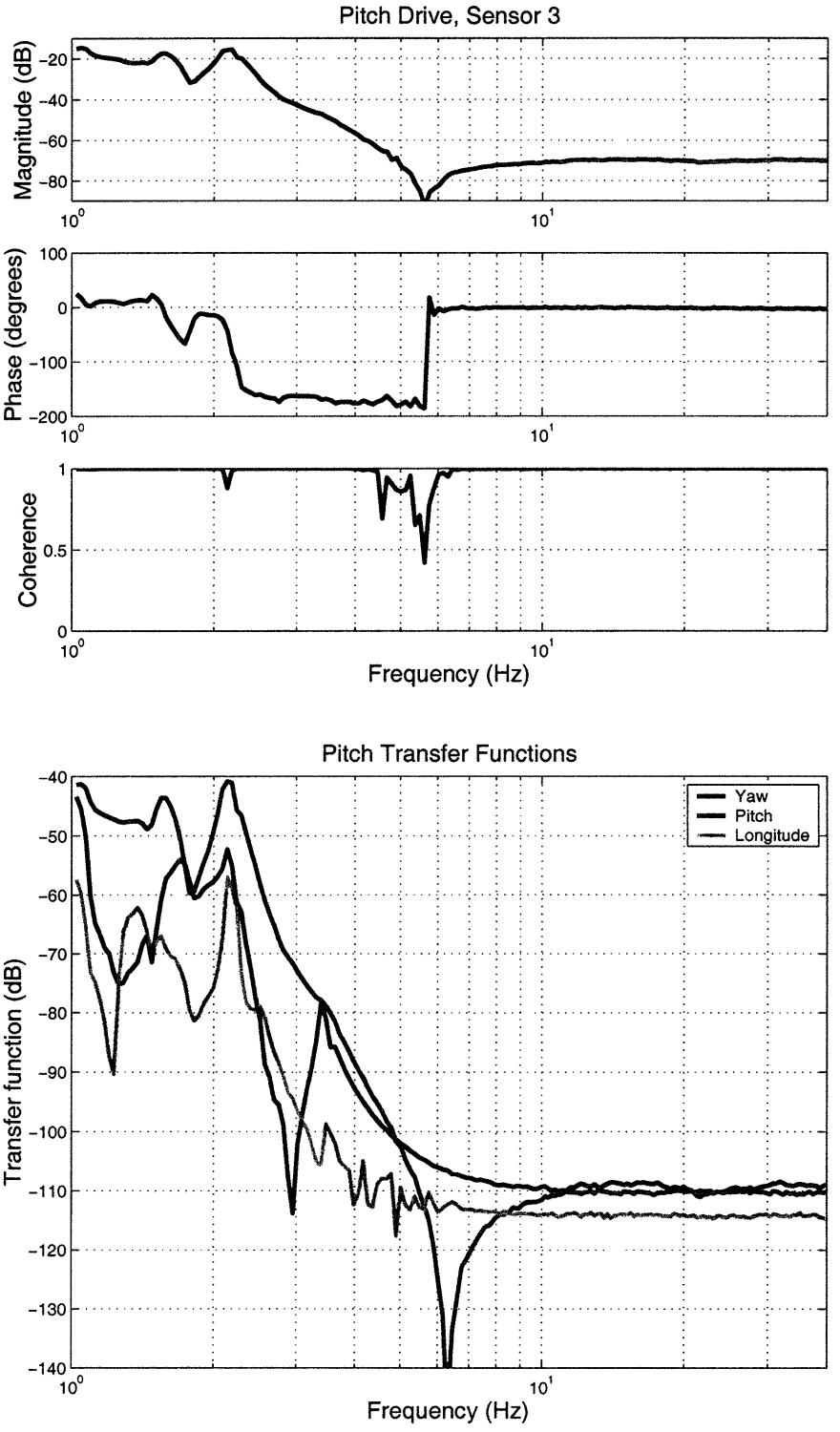

Figure 3-6: Pitch drive transfer function for sensor 3, and a graph of the transfer functions in terms of each composite mode.

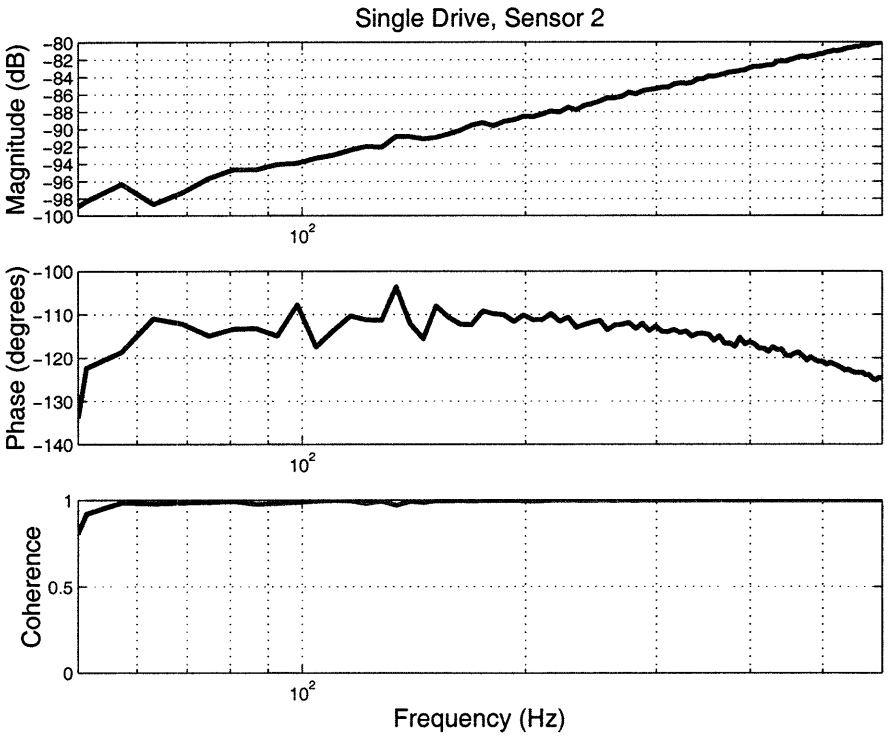

Figure 3-7: Sensor two's transfer function while the apparatus was clamped. The change in this curve is approximately 6 dB per octave, suggesting a linear dependence. This suggests an inductive effect innate to the electronics and independent of the unclamped motion.

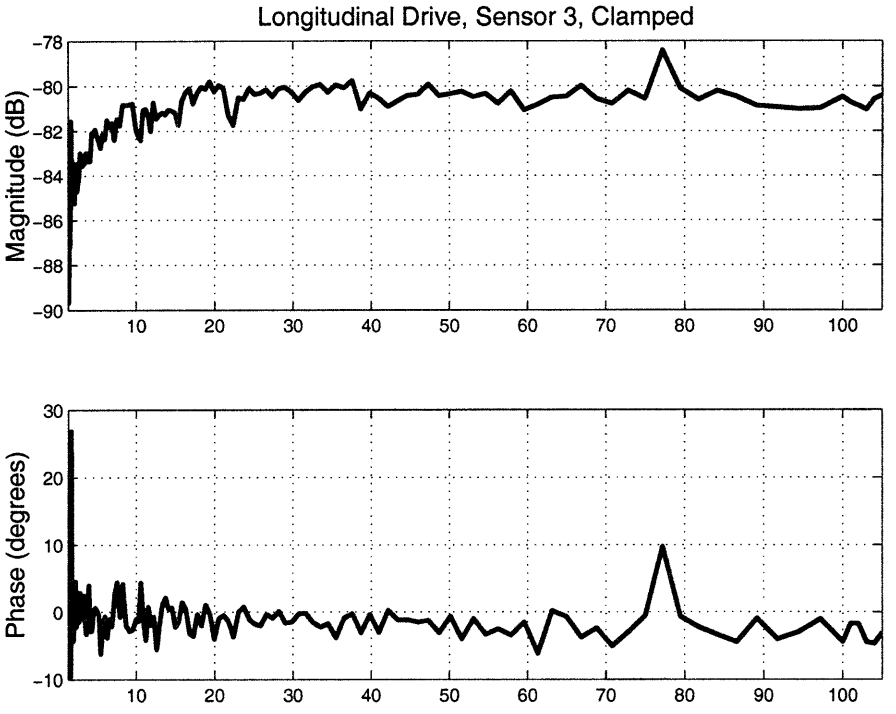

Figure 3-8: Sensor three's transfer function while the apparatus was clamped and when the third mass was driven in the longitudinal mode. The inductive effect expected from this coil pattern has disappeared.

3.3.2 Sensitivity Limit

It is clear that in all analyses taken in this experiment the transfer functions all flatten out at around -110 dB. This suggests that this value represents the characteristic noise of the position sensors themselves, and below this level the signal will be drowned.

This presents an interesting contradiction to the conclusion drawn when the apparatus was clamped and only one coil was driven. As a result, the apparatus was reclamped and the longitudinal drive applied. Perplexingly, the transfer function appears flat (see diagram 3-8) after 20 Hz. Since the longitudinal mode drives each OSEM in phase, it seems unlikely that the induction produced by each would mutually cancel. I note that this test was done with a maximum applied voltage of 1 V, as opposed to the one-coil test which had a maximum of 5 V; however, given that the magnetic field generated by the OSEM varies linearly as the applied current (and hence the applied voltage) this effect would seem to not contribute.

It therefore remains something of a mystery; when driven together, the inductive effect disappears. However, the plateau signal level when clamped is about -80 dB up to 100 Hz, which is within 3 dB of the average value for the unclamped plateau. We thus conclude, without a satisfactory explanation for the disappearing act, that the data above 10 Hz is solely a function of the electronics and not of the apparatus.

Notably, this represents a divergence from simulation data, in which there is a fall of 24 dB per octave. Since the mass we drive has two restoring forces acting upon it – the tension from the second and fourth masses – the expected f^{-4} dependence is as predicted by theory.

3.4 Comparison With Model

For comparison to theory, we make use of a programmed Simulink model, developed by Calum Torrie, of the quadruple pendulum [2]. The model breaks the resonant modes of the pendulum into four groups: longitude/pitch, yaw, vertical, and transverse/roll. The first two of these groups prove useful to our purpose. However, the model does not incorporate cross coupling between any of the groups, and so we are limited to comparing only those where the input and output in the same set.

Cross coupling between longitudinal and pitch modes would not be unexpected for even a perfect pendulum. As can be seen in graph 3-10, the pitch-driven mode frequencies line up with their expected values. These values, however, depend on the equilibrium position of the cantilever blade on the first and second masses which depends on the total mass of the third and fourth masses, and is a variable incorporated in the model. This value was tailored in the model order to identify one particular peak on the pitch-driven graphs, a change justified by the need to increase the mass of the third mass to ensure that the OSEMs were properly aligned.

3.4.1 Longitudinal vs. Longitudinal

The top panel of graph 3-9 illustrates the model and measured transfer functions of longitudinal drive and longitudinal resonance. While the expected resonance at 2 Hz,

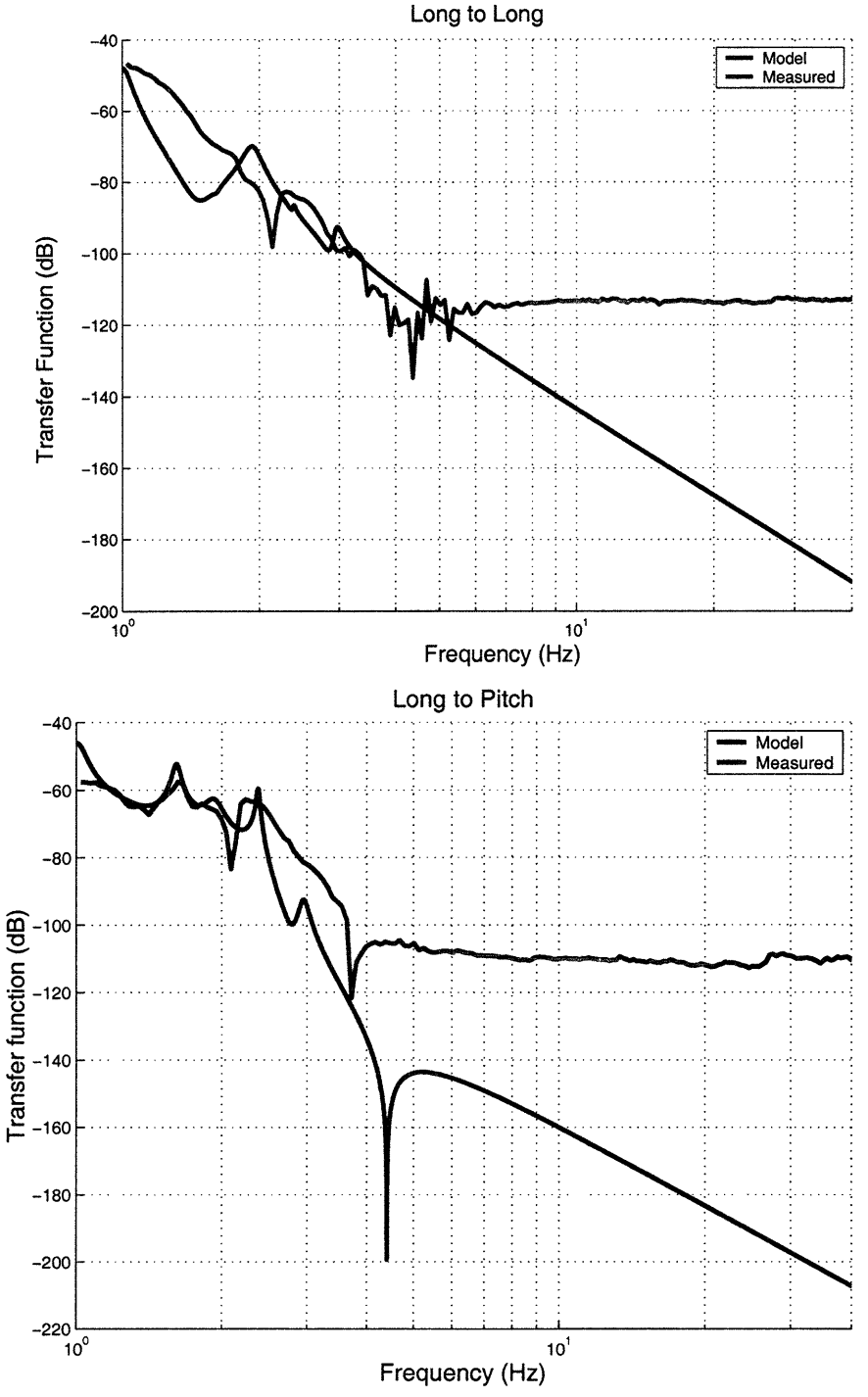

Figure 3-9: Longitudinal transfer functions, compared to the computer model prediction.

the model and measured curves are very similar from 2 to 4 Hz, with an approximate slope of 24 dB per octave, at which point the sensitivity limit is reached. An expected but small resonance at 3 Hz is mirrored by an upturn in the measured curve.

3.4.2 Longitudinal vs. Pitch

The bottom panel of graph 3-9 illustrates the model and measured transfer functions of longitudinal drive and pitch resonance. The model and measured curves are almost an exact match between 1 and 2 Hz, including a peak at 1.6 Hz. A peak expected at 2.4 Hz appears to be dulled by the presence of a zero at 2.0 Hz and is therefore inconclusive. A zero at 3.8 Hz was expected at 4.3 Hz, which is acceptable given the sensitivity of zeroes in the pitch mode and the extreme quality of the fit from 1-2 Hz.

3.4.3 Pitch vs. Longitudinal

The top panel of graph 3-10 illustrates the model and measured transfer functions of pitch drive and longitudinal resonance. A peak at 2.1 Hz is nearly exactly where predicted, and the falloff at higher frequencies lines up very nicely. A peak at 1.6 Hz appears at 1.4 Hz.

3.4.4 Pitch vs. Pitch

The bottom panel of graph 3-10 illustrates the model and measured transfer functions of pitch drive and longitudinal resonance. By lowering the model's equilibrium value of the cantilever blade position on the second mass, as explained in section 2.2.2, expected peaks at 1.6 and 2.1 Hz line up perfectly. The 24 dB per octave falloff, however, is masked by the appearance of a zero at 6 Hz; the form is only observed between 3 and 4 Hz before the extreme slope due to the zero dominates.

3.4.5 Yaw vs. Yaw

Peaks expected at 2 and 4.1 Hz appear in place, but rather than rise to a summit, there are dips where the peaks should be located.

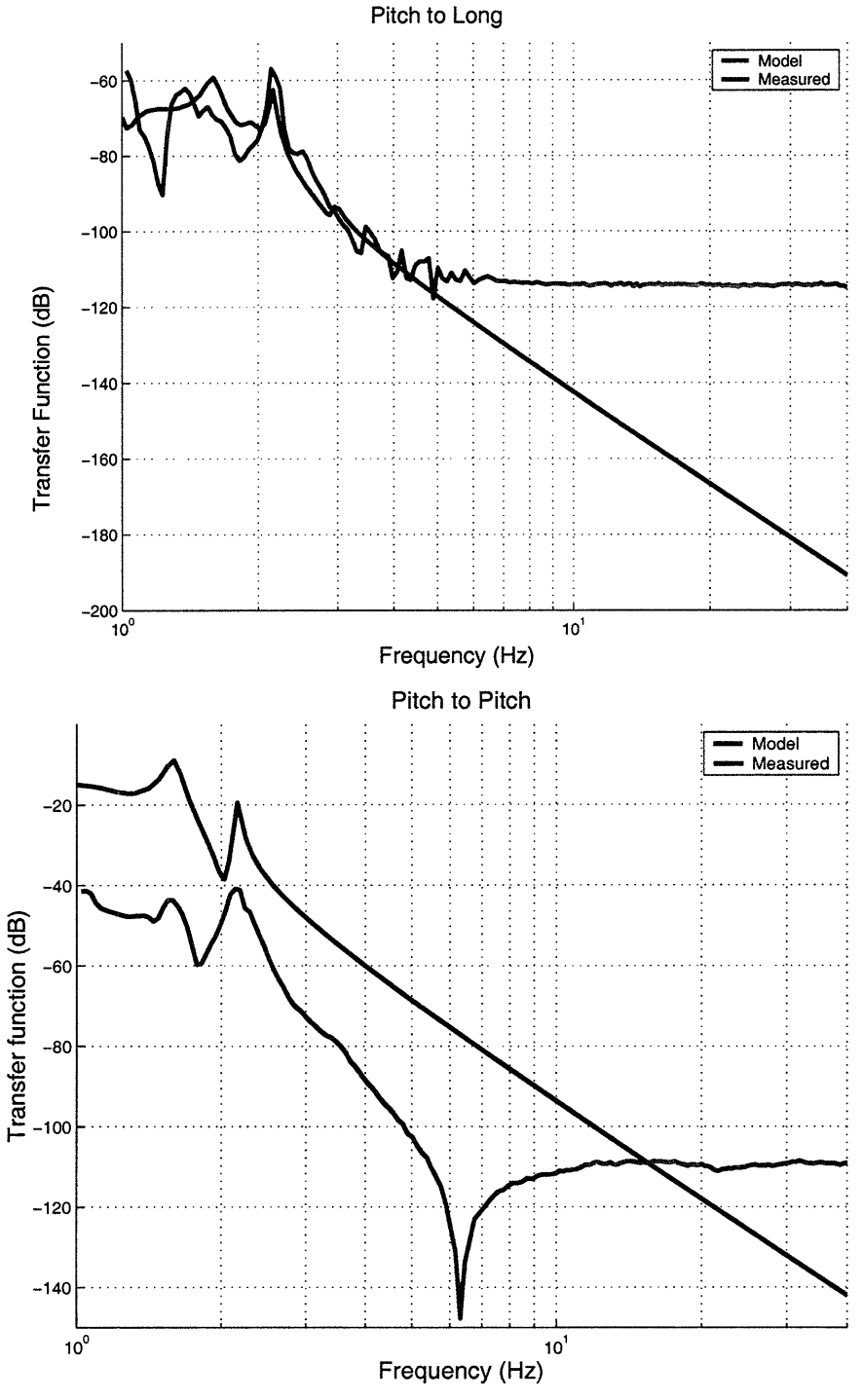

Figure 3-10: Pitch transfer functions, compared to the computer model prediction.

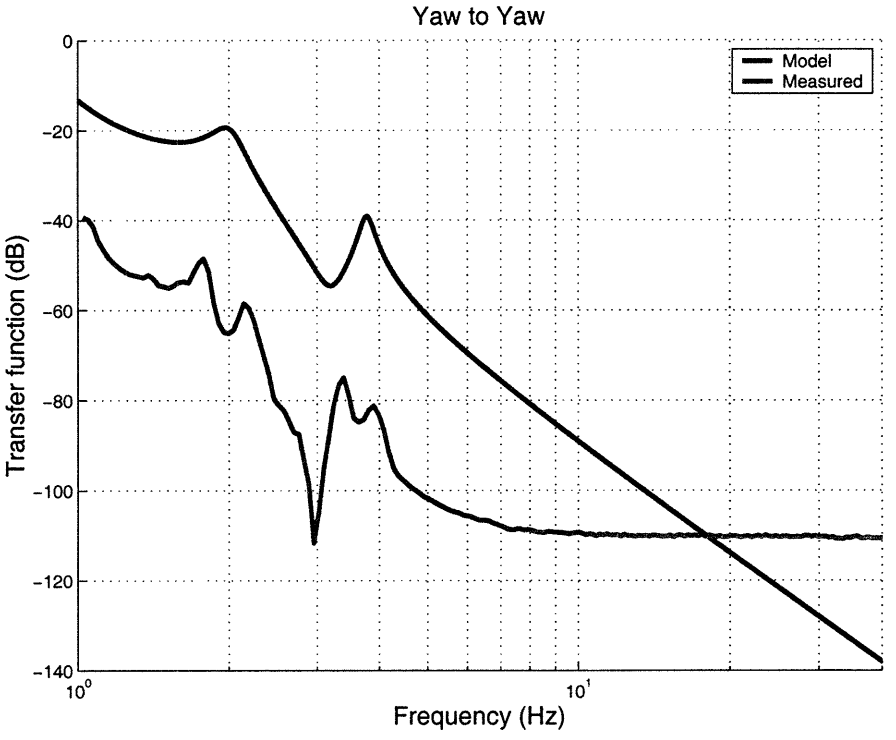

Figure 3-11: The yaw to yaw transfer function, compared to the computer model prediction.

3.4.6 Discussion

By and large, the resonant modes are where the model predicted they would be; even with mild tweaking of the model, efforts to line up one peak do not diminish the correct placement of others.

We now have an accounting for the resonant frequencies of each mode, and two in terms of different drives as confirmed by the model. We also have the hardware constructed to make the damping system. In the next chapter we discuss how we use this information and apparatus to actively damp the pendulum.

Chapter 4

Further Research

4.1 Damping system software

Active electromagnetic damping can easily be configured by using a constant drive coefficient, in a system similar to that which damps the motion of the first mass (where the relative voltage is manually configured for each coil.) However, this system can be tailored further through the use of the obtained transfer function. By analyzing the motion of the ultimate mass and choosing the coil current amplitude such that we reach the critical damping coefficient, we can ensure as little interference as possible as we bring the mass back to its equilibrium position.

Given a transfer function profile, several commercial products are available to perform this function. DSpace, among others, is well-suited to this task and is available for use. [4]

This step would be relatively painless to pursue. However, it would be of great convenience to the optical sensors that the photodetector output be amplified and rescaled. In the ambient light of the laboratory, the voltage output range is 1.22 to 1.74 V; for compatibility with the OSEMs on the first mass, this should be transformed into a voltage range of 0 to 12 V.

4.2 Refined position sensing

Sensors that are not susceptible to the close-range inductive effects of time-dependent magnetic fields are required for further measurements in this domain. The best position sensor for this task would be interferometric, though at short range a vacuum would not be required. Such sensors have already been developed by the LIGO project for other uses and could be adapted for this purpose. [5]

4.3 Closing Remarks

Seismic interference gives a clear boundary to the limits of terrestrial gravitational wave detection, and so the best way to remove this problem is to eliminate the earth from the equation. This is why future gravitational wave detectors that are on the drawing board are planned for installation in space, such as LISA (Laser Interferometer Space Antenna), a project of the European Space Agency. This apparatus is being designed to operate at frequencies that current seismic isolation technology is helpless to overcome, in the range of 10^{-4} to 10^{-1} Hz. [6] While I have no involvement in this project, I look to it with great interest.

Along with its ultimate goal of meauring gravitational waves of astrophysical origin, LIGO has been demonstrated its scientific success in that it has led to the exploration of new technologies and ideas, applicable both in this project and to others, and the ability to learn and upgrade quickly as the project progresses. This advantage is also due to a very thorough yet open-ended plan by the braintrust of the LIGO project. This experiment is a small piece in the puzzle, one that has proved to be very illuminating to me. I hope that the work I have conducted will help to drive the great project along.

Appendix A

Technical Specifications

Current Driver

Since a current source was required to power the drive system, this circuit (figure A-1) was prepared in triplicate. This allowed for a direct conversion from Siglab's voltage output to the necessary current output.

OSEMs

The LED used in each OSEM is of type SFH487, a GaAlAs high power infra-red emitting diode at a wavelength of 880 nm. The photodiode is of type BPW34, which has peak sensitivity to light of wavelength 900 nm but susceptible to light between 600 and 1050 nm. The plastic casing that holds the assembly together has an outer diameter of 3 cm and an inner diameter of 1.6 cm.

Position Sensors

The DIT-5200 Position sensors used have an output sensitivity of 20 mV/mil, or 0.79 V/mm. The sensors operate normal to an aluminum body, using changes in the induction, dependent on the position, to produce an output voltage between $\pm$ 10 V. The zero point of the sensor is about 1 mm from the object.

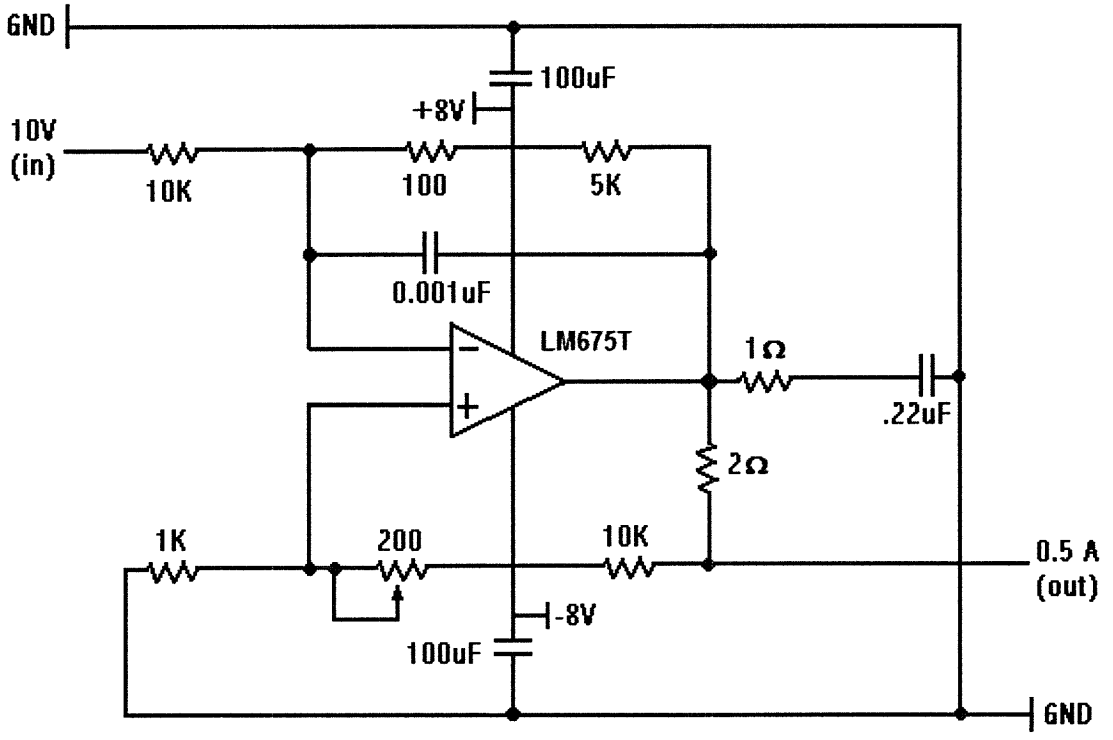

Figure A-1: The current driver circuit. Three identical drivers were constructed for parallel operation.

Bibliography

[1] E. Gustafson, D. Shoemaker, K. Strain, R. Weiss. "LSC White Paper on Detector Research and Development," LIGO Internal Document.

[2] P. Fritschel, C. Torrie, K. Strain. MATLAB Model of Quadruple Pendulum. LIGO Internal Program.

[3] Kaman Sensors Specification sheet, DIT-5200 position sensor system. http://www.kamansensors.com/html/products/pdf/wDIT-5200.pdf

[4] DSpace web site: http://www.dspace.de

[5] Malcolm Gray, David McClelland (Australian National University), Mark Barton, Seiji Kawamura (California Institute of Technology). "A simple high-sensitivity interferometric position sensor for test mass control on an advanced LIGO interferometer." http://www.anu.edu.au/Physics/ACIGA/ANU/publications/SSI.pdf

[6] LISA Gravitational Wave Observatory project summary. http://esapub.esrin.esa.it/sp/sp1219/4.2.3.lisa.qxd.pdf